Novel Digital K-Edge Imaging System with Transition Radiation from an 855 MeV Electron Beam

F. Hagenbuck, H. Backe, N. Clawiter, H. Euteneuer, F. Görgen, P. Holl, K. Johann, K.-H. Kaiser, J. Kemmer, Th. Kerschner, O. Kettig, H. Koch, G. Kube, W. Lauth, H. Matthäy, M. Schütrumpf, R. Stötter, L. Strüder, Th. Walcher, A. Wilms, C. v. Zanthier, and M. Zemter

Abstract— **A novel K-edge imaging method has been developed at the Mainz Microtron MAMI aiming at a very efficient use of the transition radiation (TR) flux generated by the external 855 MeV electron beam in a foil stack. A fan-like quasi-monochromatic hard X-ray beam is produced from the $\pm$1 mrad wide TR cone with a highly oriented pyrolytic graphite (HOPG) crystal. The absorption of the object in front of a 30 mm $\times$ 10 mm pn-CCD photon detector is measured at every pixel by a broad-band energy scan around the K-absorption edge. This is accomplished by a synchronous variation of the lateral crystal position and the electron beam direction which defines also the direction of the TR cone. The system has been checked with a phantom consisting of a 2.5 μm thick molybdenum sample embedded in a 136 or 272 μm thick copper bulk foil. A numerical analysis of the energy spectrum for every pixel demonstrates that data as far as $\pm$ 0.75 keV away from the K edge of molybdenum at 20 keV still improve the signal-to-noise ratio. Prospects are discussed to investigate the human lungs with xenon as a contrast agent at the available total primary photon flux of 2 $\times 10^{10}$/(s$\cdot$ 0.1% bandwidth (BW)) only.**

I. Introduction

THE discontinuity of the absorption coefficient at an absorption edge can be utilized to generate contrast of a heavy element embedded in a bulk material of essentially light ones. This technique is used for example in the field of medical X-ray imaging to visualize human coronary arteries. In this so-called minimum invasive digital energy subtraction angiography with synchrotron radiation (DESA) the contrast agent is iodine which is injected into the venous system. Two images are taken, one with a photon energy just above the K edge of iodine at 33.17 keV, and one with an energy just below. The iodine contrast is generated by logarithmic subtraction of the two images by which the contrast of bones and soft tissue is largely reduced. This minimum invasive technique is much less risky than the conventional coronary angiography in which a catheter is introduced into the arteries. Since in western countries 50% of the cases of death are due to cardiovascular diseases, worldwide research activities have been initiated to develop the DESA technique, in the USA, Germany, Japan, Russia, and France [1]-[5]. A large number of patients has already been successfully examined with the systems at the NSLS in Brookhaven and at HASYLAB in Hamburg [6], [7].

However, for a widespread use of this novel medical technique compact and low-cost radiation sources are required which can be operated in medical hospitals. Beside the development of compact synchrotron radiation sources also different X-ray production mechanisms (e.g., channeling radiation) have been discussed for DESA [8]-[11].

In addition to the efforts in the development of compact radiation sources the photon detection technique is being improved. A dual line high-purity germanium detector has been employed at the ESRF in Grenoble [5]. It is expected that in near future two-dimensional germanium arrays are available with a sufficient spatial resolution for DESA and a high photon detection efficiency at 33 keV. In addition, quite inexpensive compact linear accelerators are currently under development for fundamental research in high energy physics (e.g., the TESLA project) [12]. Based on such a scenario we felt that it might be appropriate to investigate the feasibility for DESA with transition radiation (TR) produced by $\approx$ 1 GeV electron beam which traverses an optimized stack of thin foils [13], [14]. Our approach aims at a very efficient use of the available photon flux. This can be achieved by taking advantage of the high integrated reflectivity of a highly oriented pyrolytic graphite (HOPG) crystal [15].

In this paper we describe a case study for such an imaging system. In sections II and III the basic principle of the imaging system, the experimental setup at the Mainz Microtron MAMI, measurements, and the data analysis are described. In section IV, our results are presented as obtained with a phantom consisting of copper as the bulk material and molybdenum as contrast material. Molybdenum with the K-absorption edge at 20 keV was chosen instead of iodine, since our silicon pn charge-coupled device (pn-CCD) detector of 0.27 mm active thickness has an efficiency too low for photons with an energy of 33 keV. The paper closes with a discussion examining the possibility to investigate the human lungs with xenon as a contrast agent.

II. Experimental Methods

A. Principle

The basic idea of the novel K-edge imaging system will be explained by means of the schematic experimental setup shown

This work was supported by the Deutsche Forschungsgemeinschaft DFG under contract Ba1336/1-1 and the Bundesministerium für Bildung und Forschung under contract 06 MZ 863 I TP2.

F. Hagenbuck, H. Backe, N. Clawiter, H. Euteneuer, F. Görgen, K. Johann, K.-H. Kaiser, O. Kettig, G. Kube, W. Lauth, and Th. Walcher are with the Institut für Kernphysik, Johannes Gutenberg-Universität D-55099 Mainz, Germany

P. Holl, J. Kemmer, R. Stötter, and C. v. Zanthier are with the KETEK GmbH, D-85764 Oberschleißheim, Germany

Th. Kerschner, H. Koch, H. Matthäy, M. Schütrumpf, A. Wilms, and M. Zemter are with the Institut für Experimentalphysik, Ruhr-Universität D-44780 Bochum, Germany

L. Strüder is with the MPI-Halbleiterlabor, D-81245 München, Germany

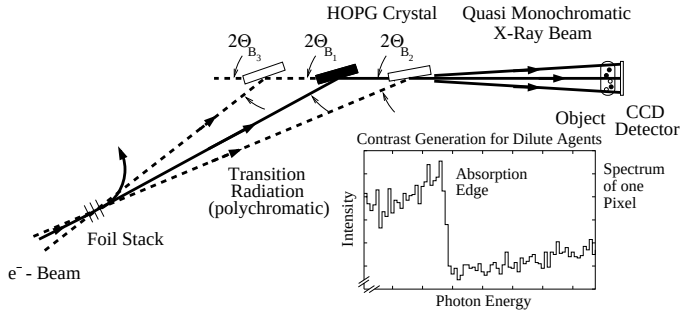

Fig. 1. Principle of the K-edge imaging system for contrast generation of dilute agents in an object. The inset shows the energy spectrum of a single pixel of the pn-CCD detector. The photon energy (abscissa) is defined by the position of the HOPG crystal at a translation stage.

in Fig. 1.

TR is generated with the 855 MeV electron beam of the Mainz Microtron MAMI in the passage of a stack of 30 polyimide foils of 25 μm thickness and spacings of 75 μm. The maximum intensity is emitted at an angle $\Theta \approx 1/\gamma = 0.6$ mrad where $\gamma = 1673$ is the Lorentz factor characterizing the electron beam energy. The energy spectrum extends up to a cutoff energy of about $\gamma\hbar\omega_P = 41.2$ keV, with $\hbar\omega_P = 24.6$ eV the plasma frequency of the foil material. A quasi-monochromatic hard X-ray beam is generated with a highly oriented pyrolytic graphite (HOPG) crystal. Quasi-monochromatic means that there exists a well-defined correlation between location and energy along the horizontal coordinate at the object in front of a pn-CCD photon detector. The object is investigated by tuning the energy at every pixel of the detector around the K-absorption edge. This is achieved by a synchronous variation of the crystal position, its angle Θ_B, and the direction of the TR cone. At such a variation the intensity distribution of the quasi-monochromatic X-ray beam remains nearly unchanged at the object.

B. Experimental Setup

The overview of the complete experimental setup at MAMI is presented in Fig. 2.

The electron beam traverses the foil stack and is bent towards the beam dump with a dipole magnet. The TR exits the vacuum system in forward direction and hits the monochromator located in the nominal position at a distance of 7.1 m from the foil stack. The flat HOPG crystal in [002] orientation has dimensions of 50 mm $\times$ 15 mm $\times$ 1.5 mm with a mosaic spread $\alpha = 0.49°$. An intrinsic bandwidth of (94 ± 10) eV was measured with a critical absorption technique at the K-absorption edge of tin at 29.2 keV [16]. The object to be investigated is located directly in front of the detector at a distance of 3.67 m from the HOPG-crystal nominal position. The asymmetric arrangement of radiator, crystal, and detector had to be chosen because of geometrical constraints in the experimental area. It causes an additional geometrical broadening of the bandwidth which was calculated to be 66 eV. At the object the X- ray spot size amounts to 63 mm (horizontal)$\times$ 20 mm (vertical) [full width at half maximum (FWHM)].

As a detector a silicon pn-CCD with an active area of 30 mm $\times$ 10 mm, a thickness of 270 μm, and a pixel size of 150 μm $\times$ 150 μm was used [17]. Since the photon detection

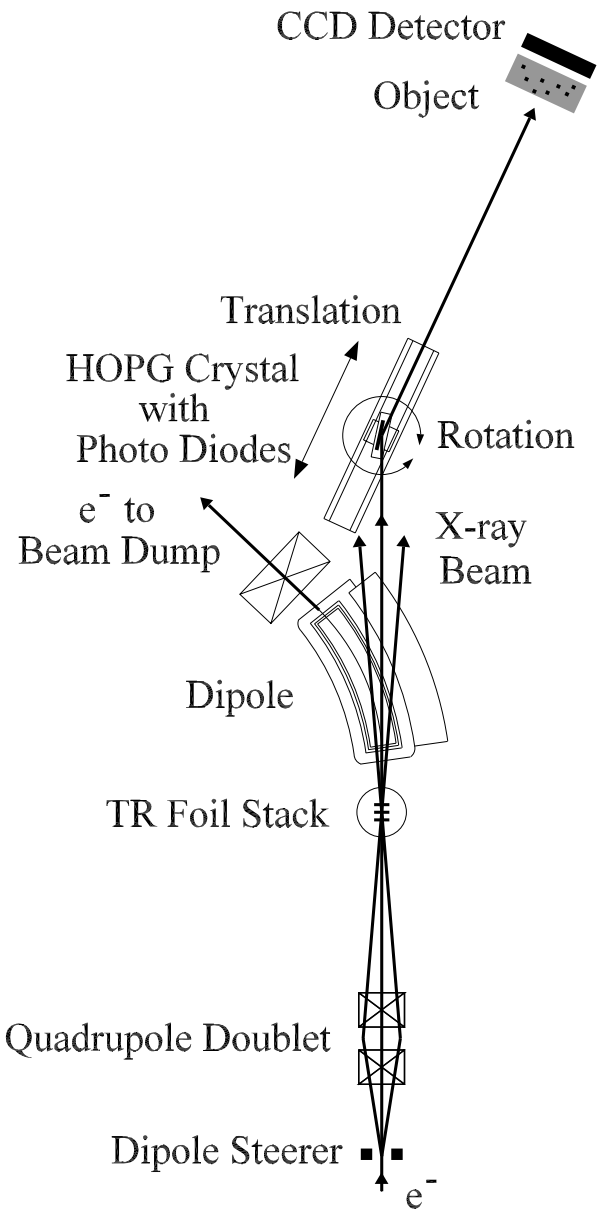

Fig. 2. Experimental setup at MAMI

efficiency of the pn-CCD drops off rapidly above an energy of 15 keV, molybdenum with the K-absorption edge at 20 keV was chosen as the contrast generating material. At 20 keV the efficiency is 24%. The corresponding Bragg angle is $\Theta_B = 5.3°$. Beside the [002] reflection at 20 keV also the [004] reflection at 40 keV is detected by the pn-CCD with an efficiency of 4%, see Fig. 5. The HOPG crystal can be moved on the translation stage with a velocity of up to 56 mm/s by a distance of $\pm$448 mm. The latter corresponds to a change of the electron beam direction of $\pm$11.5 mrad. During this shift the TR cone is kept on the center of the HOPG crystal by means of a closed-loop control system [18]. The controller, based on a digital signal processor, acts on the electron beam direction via the dipole steerer magnet , see Fig. 2. The error signal is derived from the intensity difference of two silicon photo diodes, with an active area of 2 mm $\times$ 2 mm, which are located on both sides of the HOPG

crystal at a distance of 13 mm from the center. The error signal is a measure of the direction of the TR cone which coincides with the electron beam direction.

The directional variation of the electron beam is achieved by a point-to-point imaging of the beam spot between the dipole steerer magnet and the foil stack using the quadrupole doublet. It is very important that the position of the electron beam spot at the foil stack remains nearly unchanged if the direction of the electron beam is varied. To achieve this, the horizontal beam position at the foil stack is monitored by two 9.8 GHz rf cavities which are positioned symmetrically upstream and downstream from the foil stack at a distance of 90 mm [19]. The adjustment is accomplished if the sum signal of both cavities vanishes. The full directional variation of the beam direction of ± 11.5 mrad resulted in a walk of the beam spot of about ± 6 μm only. In addition, the HOPG crystal must be turned during a scan by an angle of about $\Delta\Theta_B = 0.66^\circ$ around its vertical symmetry axis in order to keep the Bragg condition fulfilled.

The energy of the quasi-monochromatic X-ray beam was varied by this procedure at every pixel of the pn-CCD detector with a time slope of up to 185 eV/s by about $\Delta E = 2.7$ keV. The energy dispersion at the pn-CCD detector amounts to about 4.3 eV/column which corresponds to 850 eV over the total horizontal width. Both quantities vary as function of the location of the HOPG crystal and the horizontal coordinate of the pn-CCD detector, for details see Fig. 3.

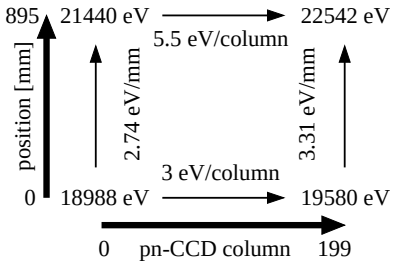

Fig. 3. Energy and dispersion at the pn-CCD detector as function of the column of the pn-CCD (lower horizontal scale) and position of the HOPG-crystal (left vertical scale). The quoted energies correspond to the indicated limits at the scales. Included are also the corresponding dispersions.

III. Measurements and Data Analysis

Experiments have been performed with a phantom consisting of a 2.5 μm thick molybdenum sample foil embedded in a 136 or 272 μm thick copper bulk foil, see Fig. 4.

Spectra were taken in the single photon counting mode of the pn-CCD detector for which an electron beam current of only 10 nA had to be chosen, far below the maximum current of

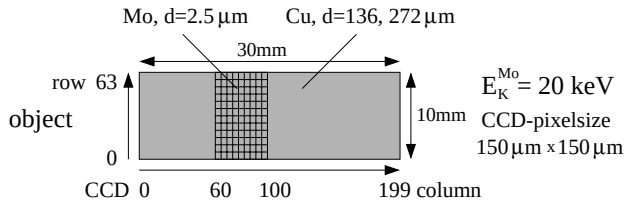

Fig. 4. Phantom used in the experiments located at a distance of 120 mm in front of the pn-CCD detector.

100 μA of MAMI. The exposure time for one frame amounted to 10 ms followed by a readout time of 5.8 ms with the beam off. While data taking the HOPG crystal was continuously moved on the translation stage with a velocity of up to 56 mm/s. The raw data of the pn-CCD were processed with a computer code developed by O. Kettig [20]. The data were corrected for different offsets and gains of the 64 on-chip amplifiers as well as for charge-transfer losses during the readout of the pixel contents. Pulse height spectra were generated this way for every pixel of the pn-CCD detector and position of the HOPG at the translation stage. For further data analysis a sliding window with a width of 1.6 keV was put in the pulse height spectra symmetrically around the center of the Bragg energy, see Fig. 5. Background originating from events in the tail of the [004] reflection at 38.8 keV, but also from cascades of high energy bremsstrahlung photons created in the foil stack and the beam dump, was subtracted from a window put above the analyzing window. With the background corrected integrated intensity, spectra were generated as function of the photon energy. The latter was determined by an energy calibration with respect to the HOPG crystal position for each column of the pn-CCD. If necessary, the intensity of a sufficient number of neighboring pixels were summed up. Examples of such spectra for the phantom shown in Fig. 4 are presented in Fig. 6(a) for a position at the pn-CCD detector with the molybdenum sample foil in front, and Fig. 6(b) only the copper foil. In Fig. 6(a) the K-absorption edge of molybdenum at 20 keV is indicated by an arrow.

Inspecting only the close neighborhood of the known K-edge energy the intensity change cannot be recognized on basis of the limited counting statistics if the included fit curve is disregarded. However, in the complete inspection interval the K edge may already be guessed. It is also evident that data very far away from the K edge become more and more insignificant. The goal of the analysis described in the following is to quantify these qualitative statements in terms of a signal-to-noise ratio (SNR)

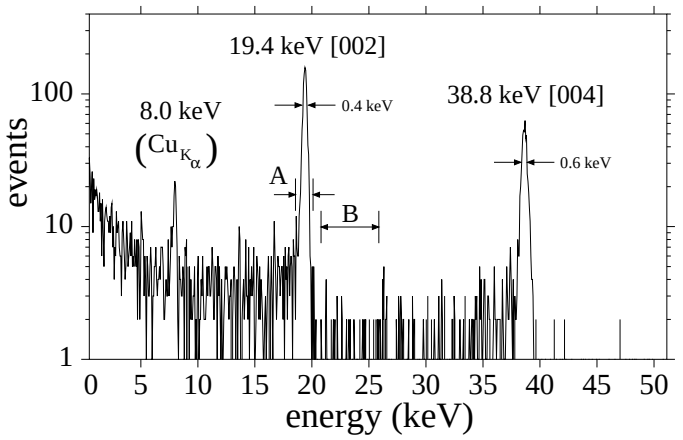

Fig. 5. Typical pulse height spectrum for column 74 and 75, cf. Fig. 4. To obtain sufficient counting statistics, 498 frames were added together, taken at the position around 50 mm of the HOPG crystal at a beam current of 10 nA. The HOPG crystal moved during the measurement by about 11 mm. This causes a line broadening of 33 eV which can be neglected. The copper K_α line originates from the bulk material of 136 μm thickness. The sliding windows on the line and for background determination are indicated by A and B, respectively.

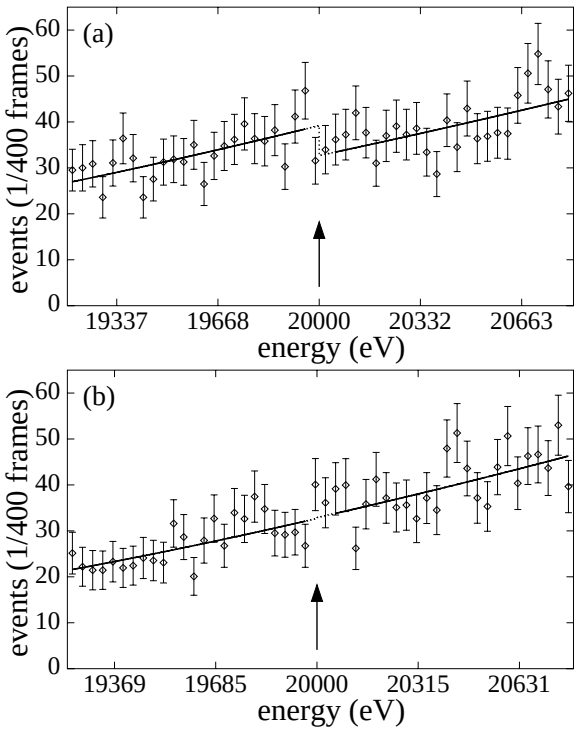

Fig. 6. Intensity as function of the photon energy for the pixel coordinates (a) 74 (column), 52 (row), (b) 12 (column), 28 (row), cf. Fig. 4. Copper foil thickness 136 μm, 2×2 pixels were added, electron beam current 10 nA, time slope of photon energy in the measurement 3.3 eV/s. The solid lines represent the independent fits with (1) above and below the K edge of molybdenum. The extrapolation to 20 keV is indicated by the dotted lines. Fit results for Mo thicknesses are for (a) (2.56 ± 1.26) μm and for (b) (-0.08 ± 1.30) μm.

which will be investigated as function of the inspection interval. For that purpose the thickness of the molybdenum sample foil has been determined by two independent best fits, one below and one above the K-absorption edge with functions

$$I(E) = a \cdot e^{-\frac{b}{E^3}} \cdot (1 - e^{-\mu_{Si}(E) \cdot d_{Si}}) \qquad (1)$$

excluding a small interval of ± 50 eV just at the K edge. The exponential takes into account the mean energy dependence of the linear absorption coefficient of copper and molybdenum ($\mu_{abs}(E) \propto 1/E^3$) which is dominated in the energy region around 20 keV by the photo effect. By the expression in parentheses the detection efficiency of the pn-CCD detector was taken into account with $\mu_{Si}(E)$ the total absorption coefficient and d_{Si} the active thickness. The known fit parameters a and b allow an extrapolation toward the K-edge energy resulting in the intensities $I(E_<)$, $I(E_>)$ for the fits in the lower and upper interval, respectively. Together with the known absorption coefficients $\mu_{Mo}(E_<)$, $\mu_{Mo}(E_>)$ of molybdenum below and above the K-absorption edge, respectively, the thickness

$$d_{Mo} = \frac{lnI(E_<) - lnI(E_>)}{\mu_{Mo}(E_>) - \mu_{Mo}(E_<)} \qquad (2)$$

of the molybdenum sample foil was calculated.

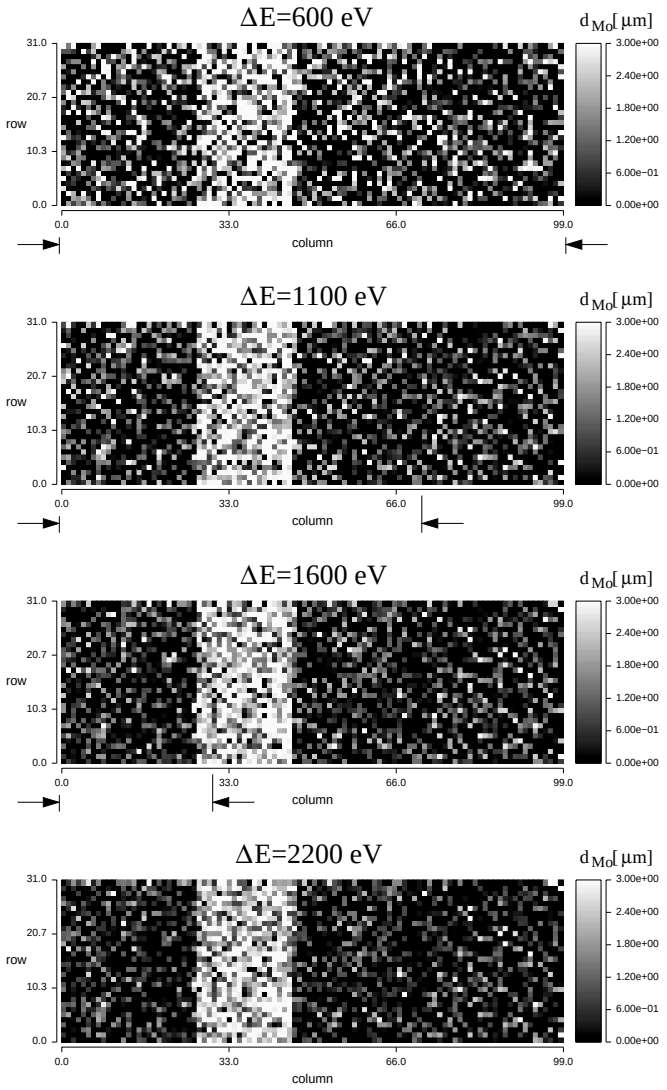

Fig. 7. Images of the phantom, shown in Fig. 4, with a 136 μm thick copper bulk foil in a gray-level representation of the fitted molybdenum thickness. Negative molybdenum thicknesses are put to zero. 2×2 pixels are combined to a new pixel of a size of 300 μm $\times$ 300 μm. From above to below the width of the fitting interval around the K-absorption edge of molybdenum has been varied as indicated by ΔE. The fit interval is symmetrical with respect to the K edge in the domain indicated by the arrows, outside asymmetrical. In the lower image the fit interval is always asymmetrical. Contrast values can be taken from Fig. 9, curve (a) for the corresponding ΔE.

IV. Results and Discussion

The results of the molybdenum thicknesses, obtained as described in the previous section, are shown in Figs. 7 and 8 in gray-level representation with the fit interval as a parameter. The contrast of the molybdenum sample improves if the analyzing interval ΔE is increased, see Fig. 7.

Finally, we address to the question from which energy interval ΔE the optimum information on the thickness of the molybdenum sample foil may be extracted. In order to quantify this question a signal-to-noise ratio $SNR = \overline{d_{Mo}}/s$ is defined from individual thicknesses d^i_{Mo} of N = 416 pixels which are covered by the molybdenum foil. This is the ratio of the mean thickness $\overline{d_{Mo}} = \sum_{i=1}^{N} d^i_{Mo}/N$ and the standard deviation

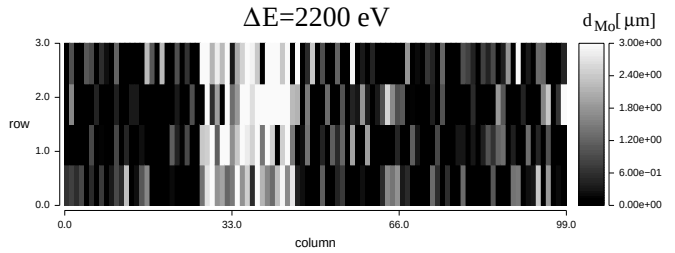

Fig. 8. Image of the phantom, shown in Fig. 4, with a 272 μm thick copper bulk foil in a gray-level representation of the fitted molybdenum thickness. Negative molybdenum thicknesses are put to zero. Because of the poor counting statistics 16×2 pixels are combined to a new pixel of 2.4 mm $\times$ 0.3 mm size.

$s = [\sum_{i=1}^{N}(d_{Mo}^{i} - \overline{d_{Mo}})^2/(N-1)]^{1/2}$. The result is shown in Fig. 9. The SNR improves steadily with increasing energy interval ΔE. Even data far away from the K edge still carry some information on the sample foil. However, above $\Delta E = 2.2$ keV the SNR is close to saturation. Therefore, it is not appropriate to choose an energy interval ΔE much larger than about 1.5 keV, since at larger ΔE the absorbed dose in the bulk material increases linearly at a slight improvement of the SNR.

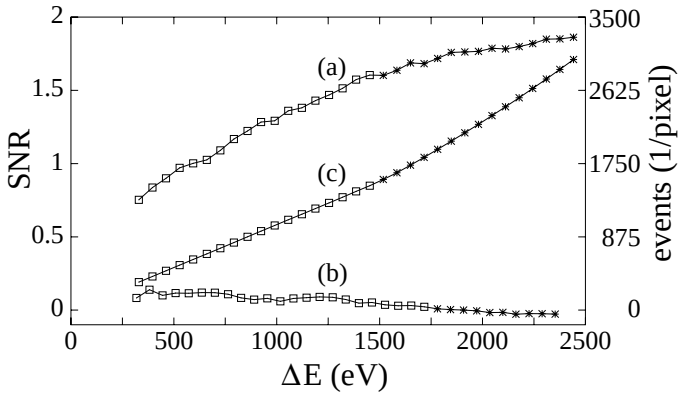

Fig. 9. SNR as derived from 416 pixels for a domain (a) covered and (b) not covered by the molybdenum sample foil. Curve (c) represents the number of photons in the energy interval ΔE. Squares (□) indicate symmetrical fit intervals with respect to the K edge, asterisks (∗) asymmetrical ones.

V. Conclusion and Outlook

Experiments which demonstrate the feasibility of a novel digital K-edge imaging system with a transition radiation source have been described in this paper. The basic components are a foil stack in which an external 855 MeV electron beam produces hard X-ray transition radiation, a tunable HOPG monochromator, and a 2-D photon detector in front of which the object under investigation is located. The system exploits the limited number of photons in a very efficient manner. This system could be of interest for a number of applications in material sciences and biology but may already be suited for medical applications, as will be demonstrated in the following.

It has been shown that the human lungs can be investigated in a quite similar manner as the human heart with the DESA technique [21], [22]. While in the latter iodine is used as a contrast agent, xenon with its K-absorption edge at 34.56 keV is used in the K-edge dichromographic bronchography. The patient inhales a mixture of 80% xenon and 20% oxygen and keeps it in his lungs for about 5 s. For DESA a photon flux of $2.7 \times 10^{11}/(\text{s mm}^2)$ in a bandwidth of 163 eV is required to yield a SNR=5 for a 1 mm thick artery employing the two-line detectors of [23]. The imaging of an area of 125 mm $\times$ 125 mm requires a total number of 6.8×10^{12} photons in the 250 ms exposure time. Since the xenon concentration is lower by about a factor of two than that of iodine, the same SNR is obtained for bronchi of 2.5 mm inner diameter. However, instead of the very short exposure time of 250 ms for DESA the exposure time for bronchial imaging may be as long as 5 s which implies a big reduction of the required photon flux. At the maximum electron beam current $I = 100$ μA of MAMI a photon flux of $2 \times 10^{10}/(s \cdot 0.1\%\ BW)$ is emitted into a ± 0.7 mrad radiation cone. This number has been calculated for a stack of 30 diamond foils with a thickness of 20 μm, a separation of 65 μm, and an average electron beam divergence of 0.22 mrad (1σ). With a flat HOPG with dimensions covering the radiation cone of ± 0.7 mrad and a mosaic spread of $\alpha = 0.49\,^{\circ}$, the X-ray spot size at the detector position amounts to 125 mm $\times$ 21 mm. A symmetrical arrangement of X-ray source, HOPG crystal, and the 2-D resolving photon detector with equal distances of 7.3 m has been assumed. The mean photon flux amounts to $3.3 \times 10^{8}/(\text{s mm}^2)$. Taking into account that our broad band energy scan with $\Delta E = 1.5$ keV is about a factor of 2.5 more efficient than the conventional dichromatic technique, a total photon number of 1×10^{13} is available in the exposure time of 5 s. Comparing with the required total number it can be concluded that, in principle, the lungs can be investigated. However, a detailed feasibility study is required to gain more insight in the various problems of such an experiment.

Acknowledgment

We gratefully acknowledge the help of D. Schroff in the course of the experiments.

References

[1] E. Rubenstein et al., "Synchrotron radiation coronary angiography with a dual-beam, dual-detector imaging system," *Nucl. Instr. and Meth. in Phys. Res. A*, vol. 291, pp. 80–85, 1990.

[2] W.-R. Dix et al., "Coronary angiography using synchrotron radiation - studies in human subjects with the system NIKOS II," *Nucl. Instr. and Meth. in Phys. Res. A*, vol. 314, pp. 307–315, 1992.

[3] A. Akisada et al., "An attempt at coronary angiography with a large size monochromatic SR beam," *Nucl. Instr. and Meth. in Phys. Res. A*, vol. 246, pp. 713–718, 1986.

[4] E.N. Dementyev et al., "First results of experiments with a medical one-coordinate X-ray detector on synchrotron radiation of VEPP-4," *Nucl. Instr. and Meth. in Phys. Res. A*, vol. 246, pp. 726–730, 1986.

[5] H. Elleaume et al., "Instrumentation of the ESRF medical imaging facility," *Nucl. Instr. and Meth. in Phys. Res. A*, vol. 428, pp. 513–527, 1999.

[6] W. Thomlinson et al., "First operation of the medical research facility at the NSLS for coronary angiography," *Rev. Sci. Instr.*, vol. 63, no. 1, pp. 625–628, 1992.

[7] W.-R. Dix et al., "Intravenous coronary angiography with synchrotron radiation at HASYLAB," *Nucl. Phys. A*, vol. 654, pp. 1043c–1046c, 1999.

[8] H. Wiedemann, M. Baltay, R. Carr, M. Hernandez, and W. Lavender, "A compact radiation source for digital subtractive angiography," *Nucl. Instr. and Meth. in Phys. Res. A*, vol. 347, pp. 515–521, 1994.

[9] F. Brinker et al., "ARI - a storage ring for non-invasive coronary angiography," *Proceedings of EPAC 2000, Vienna, Austria*, pp. 610–612, 2000.

[10] R. Carr, "Exotic sources of X-rays for iodine K-edge angiography," *Nucl. Instr. and Meth. in Phys. Res. A*, vol. 347, pp. 510–514, 1994.

[11] C.K. Gary et al., "Noninvasive digital energy subtraction angiography

with a channeling radiation X-ray source," *Med. Phys.*, vol. 20, no. 5, pp. 1527–1535, Sept/0ct 1993.
[12] R. Brinkmann, G. Materlik, J. Rossbach, and A. Wagner (editors), "Conceptual design of a 500 GeV e+e- linear collider with integrated X-ray laser facility," *DESY, Hamburg*, 1997.
[13] V.L. Ginzburg and I.M. Frank, "Radiation of a uniform moving electron due to its transition from one medium into another," *J. Phys.*, vol. 9, pp. 353–362, 1945.
[14] H. Backe et al., "Resonant transition radiation in the X-ray region from a low emittance 855 MeV electron beam," *Z. Phys. A*, vol. 349, pp. 87–92, 1994.
[15] A. K. Freund, "Mosaic crystal monochromators for synchrotron radiation instrumentation," *Nucl. Instr. and Meth. in Phys. Res. A*, vol. 266, pp. 461–466, 1988.
[16] K. Johann, "Aufbau eines Monochromators für 33 keV Röntgenstrahlung am 855 MeV Elektronenbeschleuniger MAMI," *Diplomarbeit, Institut für Kernphysik, Mainz*, 1995, unpublished.
[17] H. Soltau et al., "Performance of the pn-CCD X-ray detector system designed for the XMM satellite mission," *Nucl. Instr. and Meth. in Phys. Res. A*, vol. 377, pp. 340–345, 1996.
[18] F. Görgen, "Entwurf und Aufbau eines Kristallmonochromators für harte Röntgenstrahlung am Elektronenstrahl des Mainzer Mikrotrons," *Diplomarbeit, Institut für Kernphysik, Mainz*, 1997, unpublished.
[19] T. Doerk, "Entwurf und Erprobung einer Anordnung zur kontinuierlichen und hochauflösenden Messung der Endenergie des Mainzer Mikrotrons MAMI," *Diplomarbeit, Institut für Kernphysik, Mainz*, 1996, unpublished.
[20] O. Kettig, "Entwicklung und Test eines Röntgeninterferometers auf der Basis von Übergangsstrahlung," *Dissertation, Fachbereich Physik, Universität Mainz*, 2000.
[21] E. Rubenstein, J.C. Giacomini, H.J. Gordon, J.A.L. Rubenstein, and G. Brown, "Xenon K-edge dichromographic bronchography: synchrotron radiation based medical imaging," *Nucl. Instr. and Meth. in Phys. Res. A*, vol. 364, pp. 360–361, 1995.
[22] J.C. Giacomini et al., "Bronchial imaging in humans using xenon K-edge dichromography," *Nucl. Instr. and Meth. in Phys. Res. A*, vol. 406, pp. 473–478, 1998.
[23] T. Dill et al., "Intravenous coronary angiography with synchrotron radiation," *Eur. J. Phys.*, vol. 19, pp. 499–511, 1998.